Energy Proceedings
Vol 33, 2023
ISSN 2004-2965

Quantitative Characterization of CO2 Storage Mechanisms in Low-permeability Reservoirs

Li Jiehan[1],Jin Songhe [2] Liao Xinwei[1*]

1 China University of Petroleum, Changping District, Beijing, China.

2 Oil Production Engineering Research Institute of petrochina Daqing Oilfield Co. LTD,Da Qing,Hei Longjiang,China.
(*Corresponding Author: xinwei@cup.edu.cn)

ABSTRACT

CCUS is widely seen as a practical solution to the challenge of rising global temperatures. Enhanced oil recovery (EOR) using CO_2 flooding, as part of CCUS, can achieve both long-term geological sequestration of greenhouse gases and improved crude oil recovery, bringing significant economic benefits. In a low-permeability field, long-term water flooding is no longer able to achieve good oil recovery results, and CO_2 flooding methods are then adopted. Previous studies on CO_2 storage in reservoirs have often used qualitative and static characterization methods for CO_2 storage mechanisms. In this paper, based on the CO_2 storage mechanisms in depleted reservoirs, a method for characterizing the CO_2 storage mechanisms in low-permeability reservoirs is developed through quantitative characterization and dynamic analysis of the key parameters of the four storage mechanisms. A low permeability reservoir mechanism model is established, and the various characteristics of the four storage mechanisms with time and space as well as the distribution law are analyzed. Through this study, it can be concluded that structural and stratigraphic trapping and residual gas trapping are the main CO_2 storage methods in low permeability reservoirs, while non fluid gas in the reservoir is the main contributor to residual gas trapping. In the later stage of storage, some CO_2 is converted into residual gas in the reservoir. The effect of dissolution trapping is poor, and the influence of mineralization reaction on reservoir porosity in low permeability reservoirs is relatively small.

Keywords: CCUS, Low permeability reservoirs, CO_2 storage mechanisms, Quantitative analysis, Evolution patterns

NONMENCLATURE

Abbreviations	
APEN	Applied Energy
Symbols	
n	Year

1. INTRODUCTION

As the impact of rising global temperatures on the natural environment and human economies becomes more pronounced[1] The capture, utilization and storage of CO_2 is becoming increasingly important.[2,3] EOR and carbon sequestration is an important tool for CO_2 storage, as it not only improves oil recovery but also reduces CO_2 emissions.[4–7] Low permeability reservoirs account for 60-80% of the main body of proven geological reserves [8] and are currently the main target for CO_2 sequestration. Due to the low permeability and poor physical properties of low-permeability reservoirs, there are challenges in the research of CO_2 storage mechanisms.

The mechanisms of CO_2 storage in oil reservoirs are classified as structural and stratigraphic trapping, residual gas trapping, dissolution and mineral trapping.[9] Most studies characterize all four storage mechanisms simultaneously to obtain more accurate numerical simulation models. And they are mostly qualitative analyses.[10–12] Structural and stratigraphic trapping has been investigated in the CO_2 plume and pressure variations. The CO_2 plume was monitored at the Ketzin geological storage test site in Germany[13], the Pembina field in Canada[14] and the Frio experiment in Texas[15]. And the CO_2 plume transport was predicted based on a potential spatial mapping framework with

This is a paper for International CCUS Conference 2023 (ICCUSC2023), April 14-15, 2023, Beijing, China.

deep learning by Fan et al.[16] In the In Salah and Sleipner, respectively; Deflandre et al. applied InSAR satellite imaging and 4D seismology to monitor pressure changes during CO_2 storage[17] and Zheng et al. predicted cap pressure changes due to rapid increase in injection and partial reservoir fluid non-outflow.[18] . The mechanism of residual gas trapping has been studied by experimental and numerical simulation methods, Geistlinger et al.[19] and Krishnamurthy et al.[20] improved the capillary trapping experiment, Ren et al.[21] and Ni et al.[22] used Leverett j functions and macroscopic percolation to simulate capillary pressure fields, respectively. The dissolution mechanism has been studied to describe the dissolution-diffusion-convection process.[23–25] Mineral trapping is mostly improved characterization models in numerical simulation methods due to their long duration of action and the number of water-rock reactions to be considered.[26,27] In terms of quantifying the storage mechanism of mineral trapping, Xu et al.[28] used TOUGHREACT software to analyze and calculate the mass transfer between sandstone and shale formations and the amount of CO_2 precipitation, and Klein et al.[29] combined geochemical and reservoir simulations to calculate long-term mineralization inventory.

Based on the current state of research on the four storage mechanisms mentioned above, it can be observed that few studies have used quantitative methods to characterize the storage mechanisms. At the same time, the quantitative analysis of one of the storage mechanisms has neglected the evolution of the four mechanisms. This paper aims to propose a quantitative characterization method for CO_2 storage mechanisms in low-permeability reservoirs and to analyze the evolution of the four storage mechanisms with temporal and spatial variations.

2. MODEL BUILDING

2.1 Numerical simulation model

A three-dimensional symmetric mechanistic model is established based on the underlying physical parameters of a low-permeability reservoir. The model has a rectangular grid size of 12×12×10, with a grid of 175m in the I and J directions and 55m in the K direction. The reservoir is located 750m below the surface, with a thickness of 550m and a horizontal length of 2100m. The model is homogeneous and horizontal, with no outflow conditions at the boundary. It is assumed to be 53.1 ℃ homogeneous isothermal conditions with a rock compression factor of 3.5×10^{-4} MPa^{-1}. One injection well and one production well are set, due to the symmetry of the CO_2 plume set at the edge of the model, as shown in Figure 1. The CO_2 injection well is set at a flow rate of 8×10^5 m^3/d injected for 25 years, simulating a storage time of 625 years.

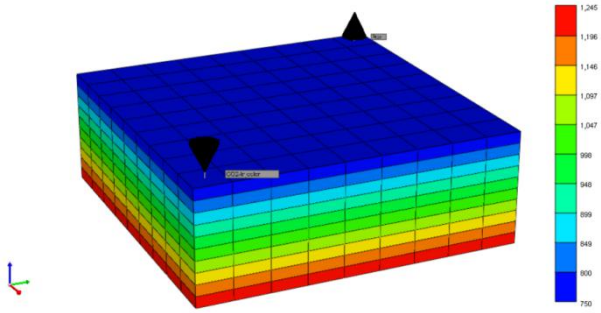

Fig. 1. The mechanistic model

2.2 Fluid model

Based on experimental PVT data from an actual low permeability reservoir, the fluids are divided into the proposed components as shown in Table 2.

The fluid density and saturation pressure were fitted by adjusting the properties of the critical temperature, critical pressure, and eccentricity factor of the proposed component of C7+. The parameter regressions resulted in a density of 0.816 g/cm^3 at formation temperature and pressure and a saturation pressure of 5.61 MPa. Relative volume change, viscosity change, crude oil formation density, and volume factor were fitted by constant mass expansion (CCE) and multiple degasifications (DL) experiments with increasing pressure. The mean error in the fitted relative volume was 0.0215% and the mean error in the fitted formation density was 0.002% in the constant mass expansion experiment, and the mean error in the fitted volume coefficient was 0.0395% in the multiple degassing experiments. The regression of the attribute parameters resulted in small errors and high fitting accuracy, which can better reflect the fluid properties of the formation.

Table 1 Basic physical properties

Basic parameters	Numerical simulation models
Average permeability (mD)	16.95
Average porosity (%)	14.67
Water content saturation (%)	58.8
Stratigraphic crude oil density (g/cm^3)	0.816
Average original stratigraphic pressure (MPa)	11.08
Reservoir temperature (°C)	53.1

Table 2 Division of pseudo components

Pseudo-components	Content (mol%)
CO_2	0.04
N_2	1.74
C1-C4	16.71
C5-C6	14.74
C7-C8	16.80
C9-C10	19.65
C11+	30.32

2.3 Mechanisms of CO_2 storage in the model

2.3.1 Residual gas trapping

The mechanistic model uses the Larsen and Skauge model to consider the oil-gas-water three-phase phase permeation hysteresis effect, and if gas saturation decreases again then a secondary replacement curve will occur. The relative permeability of the gas phase of the secondary repulsion is calculated as shown in Equation 1:

$$k_{rg}^{drain} = \left[k_{rg}^{input} - k_{rg}^{input}\left(S_g^{start}\right)\right]\left[\frac{S_{wcon}}{S_w^{start}}\right]^{\alpha} + k_{rg}^{imb}\left(S_g^{start}\right) \quad (1)$$

where k_{rg}^{drain} -- the relative permeability of the gas phase of the secondary repulsion;

k_{rg}^{input} - relative permeability of the gas phase of the primary repulsion;

$k_{rg}^{input}\left(S_g^{start}\right)$ - the relative permeability of the gas phase of the primary drive corresponding to the gas saturation at the start of the secondary drive;

S_{wcon} --initial water content saturation;

S_w^{start} --saturation of the aqueous phase at the start of the secondary replacement curve;

$k_{rg}^{imb}(S_g^{start})$ - the relative permeability of the gas phase at the start of the secondary repulsion;

α - deflator.

The term in the exponent α illustrates the gradual decrease in the relative permeability of the gas phase in the presence of flowing water, Equation 1 implies that the relative permeability of the gas phase is a function of the order of saturation of the gas and water phases.

2.3.2 Residual gas trapping

Henry's law and the Stokes-Einstein and Sigmund correlations are used to describe the dissolution and diffusion processes of CO_2 in the formation fluid.

The Henry's constant H, an important coefficient in Henry's law, can be calculated for CO_2 by using the Harvey regression equation which makes the Henry's constant a function of pressure, temperature, and salinity and is applicable up to 150°C and 70 MPa, the Henry's constant is calculated as follows:

$$lnH = lnP^s + A/T^* + B(1-T^*)^{0.355}/T^* + C\exp(1-T^*)(T^*)^{0.41} \quad (2)$$

where *H* - Henry's constant;

P^s - solvent vapor pressure;

T^s - dimensionless number, $T^s = T/T_c$;

T_c - solvent critical temperature.

When the solute is CO_2, the constant *A* in the regression equation is -9.4234, *B* is 4.0034 and *C* is 10.3199. This method of calculating Henry's constant applies to both formation water and formation crude oil. The concentration that acts in the electrolyte solution is called the effective concentration, i.e. the activity. The model uses the B-DOT model to calculate the activity coefficient for the aqueous phase.

Unlike the dissolution process, the diffusion of CO_2 in formation fluids requires separate consideration for the formation of water and the formation of crude oil. The Stokes-Einstein correlation calculates molecular diffusion in the water phase, while the diffusion model in the oil phase uses the Sigmund correlation, with the binary diffusion coefficient calculated as shown in Equation 3:

$$D_{ij} = \frac{\rho_k^0 D_{ij}^0}{\rho_k} \cdot (0.99589 + 0.096016\rho_{kr} - 0.22035\rho_{kr}^2 + 0.032874\rho_{kr}^3) \quad (3)$$

where ρ_k - the fluid density;

ρ_{kr} - the product of density and diffusivity.

2.3.3 Mineral trapping

Based on the formation water mineral ion assay and the formation rock mineral composition report, the main components of the clay minerals in the mechanism model are kaolinite, illite, chlorite, and montmorillonite, and the reaction equations involved in the mineral trapping are shown in Table 3.

Table 3 Mineralization reaction equations

Type of chemical reaction	Reaction equation
CO_2 dissolved	$H_2O \rightleftharpoons H^+ + OH^-$ $CO_2 \rightleftharpoons H^+ + HCO_3^-$ $HCO_3^- \rightleftharpoons H^+ + CO_3^{2-}$
Rock mineral	$Al_2Si_2O_5(OH)_4 + H^+ \rightleftharpoons Al^{3+} + H_2O + SiO_2$

dissolution	$K_{0.6}Mg_{0.25}Al_{2.3}Si_{3.5}O_{10}(OH)_2 + H^+ \rightleftharpoons Al^{3+} + H_2O + K^+ + Mg^{2+} + SiO_2$
	$CaCO_3{:}H_2O + H^+ \rightleftharpoons Ca^{2+} + H_2O + HCO_3^-$

3. QUANTITATIVE CHARACTERIZATION OF CO_2 TRAPPING

3.1 Structural and stratigraphic trapping

The CO_2 plume expands rapidly during the injection phase, and for 25 years since the end of the injection phase, the plume changes are dominated by lateral transport, with a more concentrated range of carbon dioxide and a smaller change in molar concentration. Over the next 75 years, the plume travels very little lateral distance but passes through more pore space, and the plume extent increases, while the CO_2 molar concentration decreases in the vicinity of the injection well, as shown in Figure 2. By 575 years of storage, the upward transport of the CO_2 plume is significant and the plume extent expands significantly, with a maximum molar fraction of 88.76% near the injection well. It is also noted that there is a large difference in CO_2 molar concentration at different distances at the start of injection. As time increased, the CO_2 molar concentration in the near-well region keeps decreasing and the concentration difference becomes smaller. The curves of CO_2 molar concentration versus distance from the injection well at different times are shown in Figure 3.

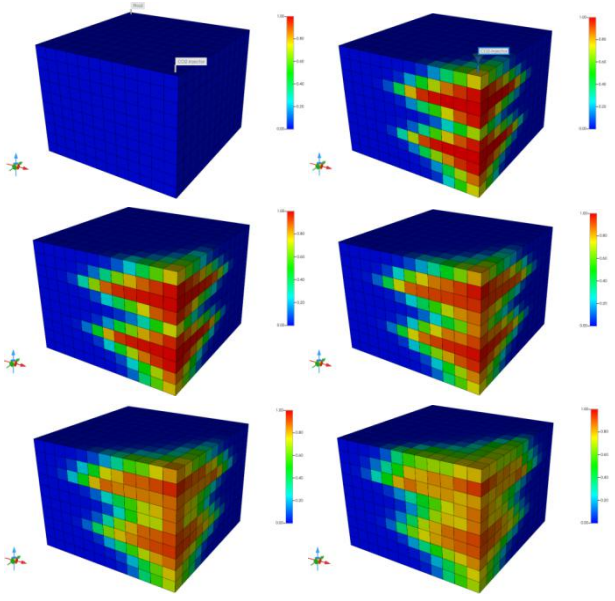

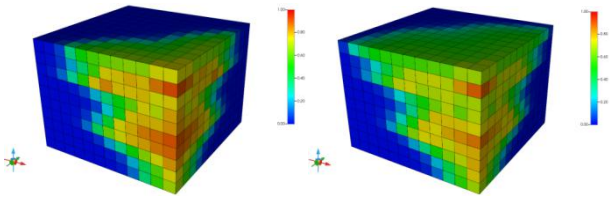

Fig. 2. CO_2 plume variation

The formation pressure in the CO_2 injection phase varies considerably, as can be seen in Figure 4. The pressure at the beginning of CO_2 injection varies considerably and reaches a maximum value of 25.3 MPa at 1135m at the end of the injection phase, which is still less than 0.95 times the rock rupture pressure of 27.35 MPa, proving the safety of the structural and stratigraphic trapping at the current daily injection volume. The pressure gradually propagates throughout the block during the storage phase, as shown in Figure 5, with an overall decrease in formation pressure during the storage period of 575 years and a maximum formation pressure of 11.75 MPa at the end of the simulation.

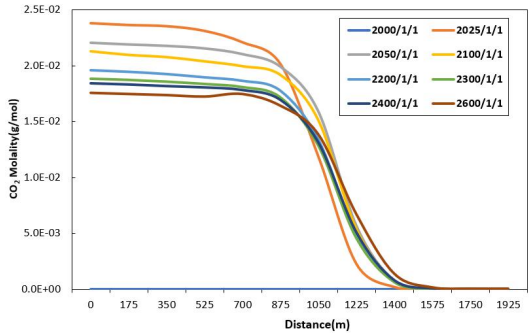

Fig. 3. CO_2 molar concentration versus distance

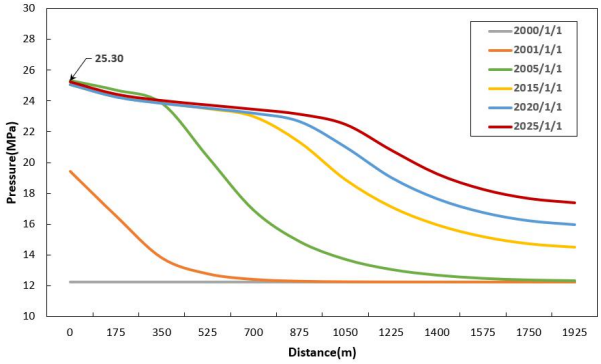

Fig. 4. Pressure curves with distance from injection well

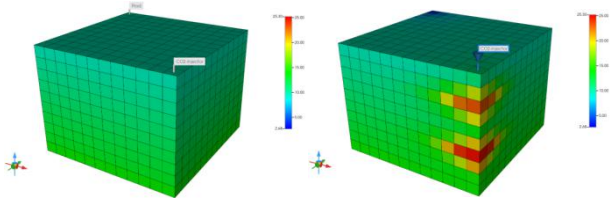

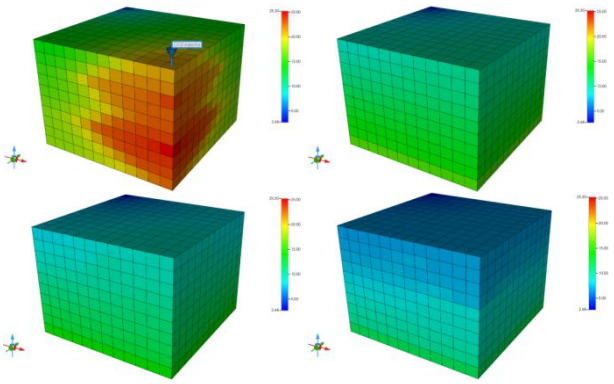

Fig. 5. Pressure distribution at different times

3.2 *Residual gas trapping*

The volume of residual gas trapping is divided into two parts, one is the phase seepage hysteresis capture and the other is due to the gas-bearing saturation being lower than the residual gas saturation, i.e. non-flowing gas in the formation. The non-flowing gas in the injection phase is distributed in a plume with the injection well as the axis and the injection point as the furthest lateral distance. The non-flowing gas content at this stage is extremely low, no more than 2%. During the storage phase, the non-flowing gas is distributed within the CO_2 plume, but gradually changes towards the top of the reservoir, while its content gradually increases overall. By the end of the storage phase, the maximum non-flowing gas content is 58%. The variation of non-flowing gas saturation in the reservoir is shown in Figure 6.

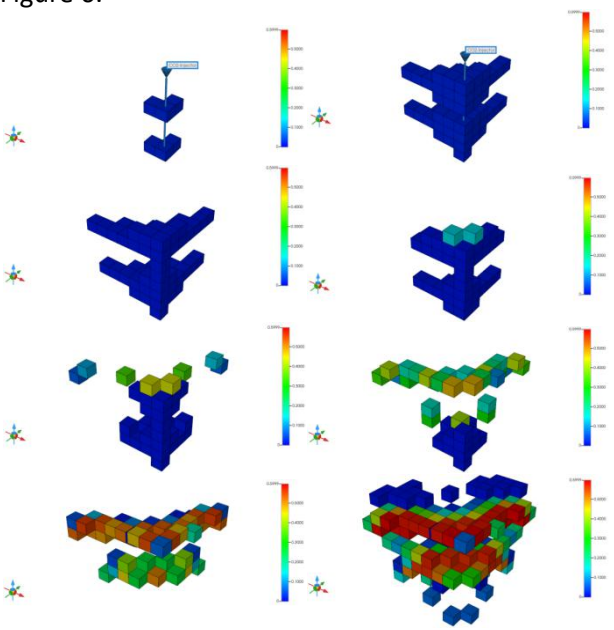

Fig. 6. Immobile gas saturation at different times

3.3 *Dissolution trapping*

Dissolved reservoir storage includes both formation water dissolution and CO_2 dissolution in crude oil. The amount of CO_2 dissolved in the formation of crude oil is more in the early stage of storage, and the amount of dissolved CO_2 in both the water and oil phases increases rapidly during the injection phase, while the amount of dissolved CO_2 in the oil phase fluctuates widely, as shown in Figure 7.

CO_2 The direction of gas flow is along the injection well and in the vertical injection well direction in the early stages of injection, with an increase in gas flow in the inclined direction in the middle and late stages of injection, along with a gradual increase in the inclination angle. In the early stages of storage, the downward flow direction along the injection wells gradually decreases, and during this period the gas flows mainly upwards along the injection wells, accompanied by some vertical outward flow, and then gradually decreases in the upward and oblique direction along the injection wells. At around 125 years of storage, the main flow direction begins to shift to the upper half of the reservoir. Around 205 years of storage, the gas flow begins to expand, and by the end of the storage phase, the direction of flow increases. CO_2 The direction of gas flow in the plume is shown in Figure 8.

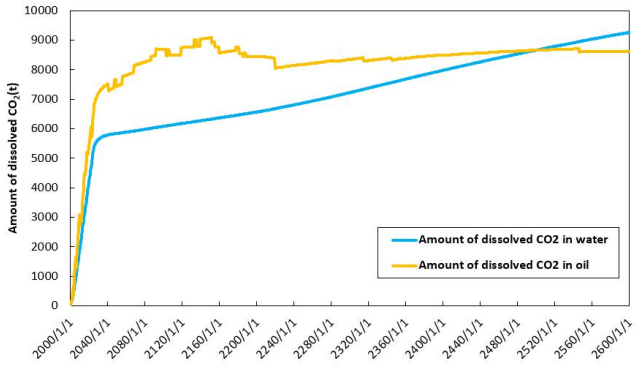

Fig. 7. Variation in dissolved amounts in the aqueous and oil phases

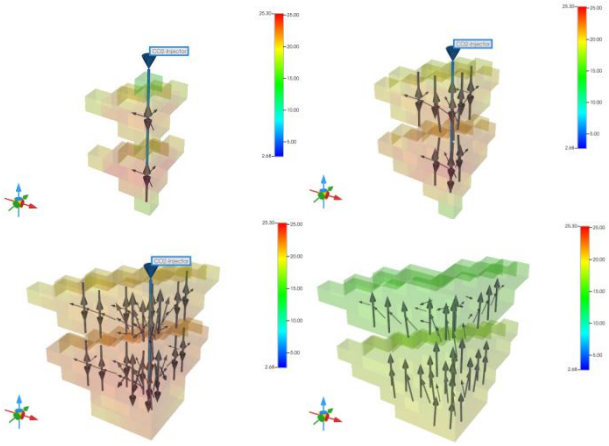

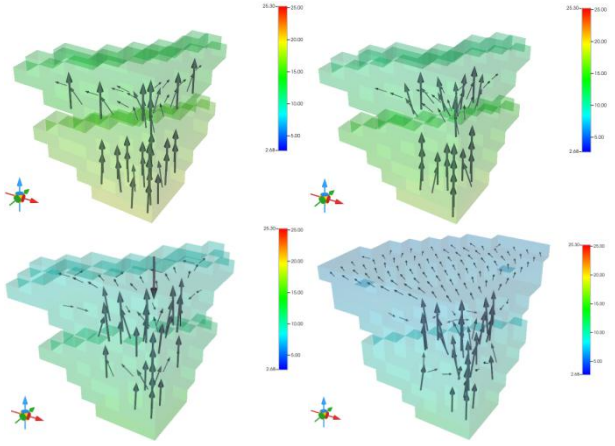

Fig. 8. Direction of gas flow at different times

During the injection phase, CO_2 contacts new formation fluids at a rapid rate, with dissolved volumes growing rapidly in both formation water and crude oil. At the end of the injection phase, the dissolved volume in the oil phase is still increasing, but the dissolution rate decreases and, combined with the change in the direction of gas flow, it can be assumed that the decrease in the upward flow direction reflects the gradual weakening of the convection process between the gas and the formation fluid, resulting in a reduction in the dissolution-diffusion-convection cycle. Thereafter, the direction of gas flow begins to change towards the upper part of the reservoir, reflecting the fact that at this stage CO_2 transport is mainly within the carbon dioxide plume, and contact with the formation fluids slows down, resulting in the dissolved volume in the oil phase beginning to decrease. Subsequently, the range of gas flow begins to increase and the amount of dissolved CO_2 begins to gradually increase again as it comes back into contact with the formation fluids. However, as the gas flow rate is less than the injection phase flow rate, the rate of increase in dissolved volume during this time is much less than during the injection phase.

3.4 Mineral trapping

The main carbonate deposition component in the reservoir is $CaCO_3$, whose dissolution rate is lower than its production rate, as shown in Figure 9, so the $CaCO_3$ content in the reservoir will keep increasing over time. In particular, the $CaCO_3$ content in the reservoir increases more rapidly during the injection phase, while it gradually slows down during the storage phase. At the same time, other rock minerals are gradually dissolved, resulting in a decreasing content in the reservoir.

Carbonate precipitation was first generated in the near-well area, and the precipitation content at the same distance continued to increase dynamically with time, and the extent of precipitation generation expanded with time, as shown in Figure 10. However, the change in porosity caused by the mineralization reaction is smaller and concentrated in the near-well area, as shown in Figure 11. However, the porosity variation does not exactly coincide with the extent of precipitation variation, suggesting that although the other mineral content varies to a lesser extent, it still affects the change in reservoir physical properties.

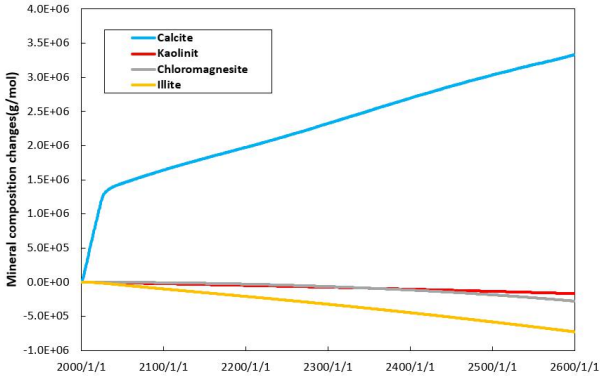

Fig. 9. Rock mineral variation curves with time

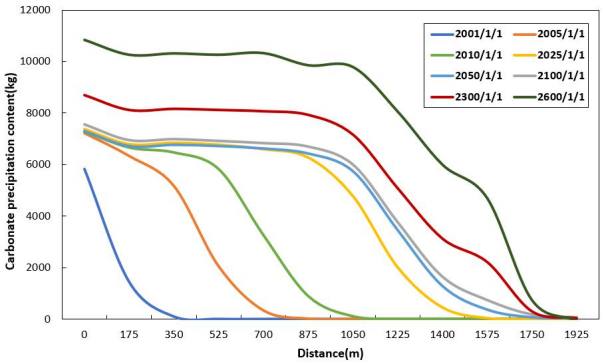

Fig. 10. Carbonate precipitation versus distance from injection well curves

3.5 Evolutionary Patterns of CO_2 storage mechanisms

Of the four storage mechanisms, structural and stratigraphic trapping and residual gas trapping contributed the majority of CO_2 storage. At the end of the injection phase, structural and stratigraphic trapping was 1.25×10^7t, residual gas trapping was 1.08×10^5t, dissolved storage was 1.2×10^4t and mineralized storage was 53.5t, while at the end of the storage phase, structural and stratigraphic trapping was 7.21×10^6t, residual gas trapping was 5.38×10^6t, dissolved storage was 1.79×10^4t and mineralized storage was 1.47×10^2t. Since the end of the CO_2 injection Since the end of CO_2 injection, the total storage volume remained at 1.26×10^7 t. 0.048% of the supercritical CO_2 was converted to ions and carbonate precipitation in water, and the main evolution of the storage mechanism was the change from structural and stratigraphic trapping to residual gas trapping.

At the beginning of the storage phase, the tectonic inventory grows slowly and is considered to be a small increase in CO_2 from the wellbore reservoir. Subsequently, the tectonic inventory begins to decline and some of the supercritical CO_2 sequestered by the structural and stratigraphic trapping is converted to non-flowing gas, which is also supercritical CO_2, but with residual gas trapping. At the same time, the CO_2 plume moves slowly laterally and vertically during this phase, but the plume extent gradually increases as can be seen in the 3D simulations. On a spatial scale, the supercritical CO_2 passes through more pore space, which is the main reason for the shift to residual gas trapping. The CO_2 plume gradually expands, but the total amount of CO_2 in the formation remains the same, its concentration gradually decreases and the formation pressure also decreases.

During the injection phase, phase seepage hysteresis trapping is the dominant mode of residual gas trapping, while non-flowing gas is the dominant mode of residual gas trapping in the middle and late stages of the storage phase. During the injection period, the formation of CO_2 continues to increase, continuously displacing the formation fluids, while the displaced formation fluids reoccupy the rock pore space, resulting in a significant phase seepage hysteresis effect. After the cessation of injection, the fluids in the formation become less mobile and the phase seepage hysteresis gradually decreases, while some of the supercritical CO_2 is dissolved in the formation water and crude oil, resulting in a slow decrease in the volume of residual gas trapping. As the CO_2 plume gradually expands and contacts new rock pores, the gas-bearing saturation decreases gradually below the residual gas saturation, increasing the distribution range and content of non-mobile gas.

The dissolution rate in the formation water decreases during the storage phase, but the dissolved amount continues to increase. The dissolved amount of CO_2 in the formation water and the mineralized storage interact with each other, and the HCO_3^- ions decomposed by dissolved gas in the formation water decrease due to the mineralization reaction to form carbonate precipitation on one side and increase due to the rising content of dissolved gas on the other side, in a dynamic equilibrium. In this paper, the role of the dissolved storage mechanism is much greater than that of mineralized storage, and the HCO_3^-, which is decomposed by dissolved gas, is much smaller than the dissolved CO_2 content, and the ion content keeps rising, as shown in Figure 12. This indicates that the evolution of supercritical CO_2 to the ionic form, although low, is expanding in proportion and requires a longer time to improve the safety of CO_2 storage.

The mineralization reaction occurs in the CO_2 plume passing through the space and is influenced by the extent of the plume and dissolved storage. During the rapid expansion of the plume in the injection phase, the $CaCO_3$ content increases rapidly. However, the ion content of the formation water increases slowly during the storage phase, which also results in a low evolution of the other three mechanisms toward mineralized storage.

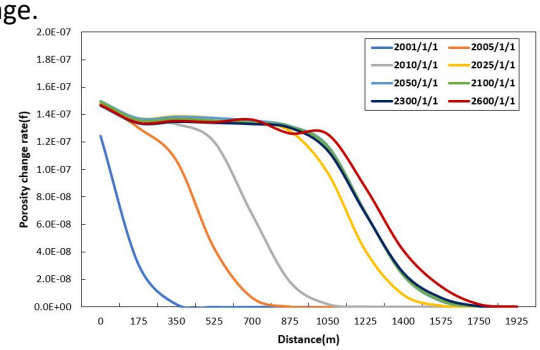

Fig. 11. Porosity versus injection well distance curves

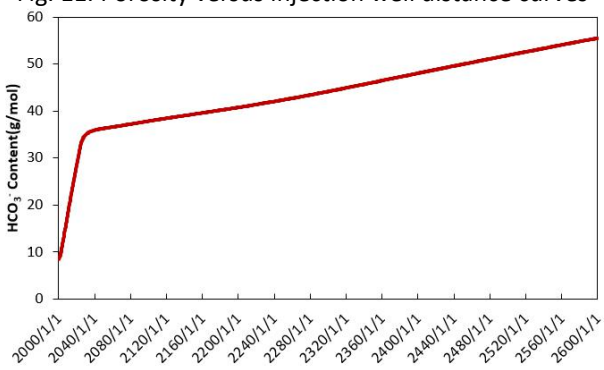

Fig. 12. Variation in HCO_3^-content in stratigraphic water

4. CONCLUSIONS

In this paper, a fluid model and mechanism model for low-permeability reservoirs are established, and key parameters are fitted to verify the reliability of the model. Based on the carbon storage mechanism of depleted reservoirs, a quantitative characterization method of carbon storage mechanism in low-permeability reservoirs is proposed, and the distribution characteristics and evolution laws of four carbon storage mechanisms are analyzed. The following conclusions were obtained:

1) In the gas injection stage, tectonic and dissolved storage contribute to the main storage volume. In the low permeability reservoir storage phase, tectonic and residual gas trapping are the dominant CO_2 storage modes;

2) Tectonic embedment is the basis for long-term,

safe sealing of CO_2 in the reservoir. The larger the extent of the CO_2 plume, the better the effect of the other three embedment mechanisms. Slow pressure propagation and rapid local pressure rise in low permeability reservoirs require monitoring of formation pressure changes in the vicinity of the injection well, as well as consideration of the relationship between well spacing and plume length;

3) Non-flowing gas in the reservoir is the main contributor to residual gas trapping and has a significant role in the middle and late stages of storage. Low longitudinal permeability in low permeability reservoirs has a poor effect on dissolved storage in the storage stage. When gas is transported mainly within the plume, this will result in a reduction in dissolved gas volumes;

4) Dissolved gas in the formation of water is the basis of the mineralization reaction, and the small amount of dissolved storage at the storage stage inevitably leads to less mineralization storage. The rate of carbonate generation and precipitation in low-permeability reservoirs is greater than the rate of dissolution, and the mineralization reaction has less impact on reservoir porosity;

5) Structural and stratigraphic trapping has been the major part of the total carbon buried, but as storage time increases, some of the CO_2 is gradually converted to residual gas in the reservoir, increasing residual gas trapping. Dissolved gas in the oil phase decreases in the later stages of storage due to pressure changes, while dissolved gas in the water phase continues to increase with time. At the same time, the amount of residual gas trapping increases slowly in the late stages of storage, and it can be predicted that if the storage time increases, the residual gas trapping in the reservoir will further switch to the dissolved storage mode. This change will also promote the occurrence of mineralization reactions and increase the amount of mineralization buried in the reservoir;

6) The carbon dioxide plume is the largest area where the four carbon storage mechanisms act. Due to the low density of supercritical CO_2, residual gas trapping occurs in the middle and upper parts of the plume. Dissolved storage is more likely to take place at the point of contact between the plume and the fluid, with the mineralization reaction occurring first in the near-well region and gradually expanding over time towards the plume boundary.

The study of the storage mechanism reveals that supercritical CO_2 is the main storage method in low-permeability reservoirs, which also poses certain challenges to the efficient and safe storage of CO_2. The results of this paper provide a reference for further research on the storage mechanism in oil reservoirs and also lay the foundation for studying the evolution of the storage mechanisms.

DECLARATION OF INTEREST STATEMENT

The authors declare that they have no known competing financial interests or personal relationships that could have appeared to influence the work reported in this paper. All authors read and approved the final manuscript.

REFERENCE

[1] HOEGH-GULDBERG O, JACOB D, TAYLOR M, et al. Impacts of 1.5°C of Global Warming on Natural and Human Systems. 138. (Reference to a journal publication)

[2] OSMAN A I, HEFNY M, ABDEL MAKSOUD M I A, et al. Recent advances in carbon capture storage and utilisation technologies: a review. Environmental Chemistry Letters, 2021, 19(2): 797-849. DOI:10.1007/s10311-020-01133-3. (Reference to a journal publication)

[3] ZHANG L, LING J, LIN M. Carbon neutrality: a comprehensive bibliometric analysis. Environmental Science and Pollution Research, 2023, 30(16): 45498-45514. (Reference to a journal publication)

[4] WANG P, WU X, GE G, et al. Identification of potential CCUS clusters and its pipeline network optimization in China[J/OL]. E3S Web of Conferences, 2022, 358: 02015. (Reference to a journal publication)

[5] LI X Y, GAO X, XIE J J. Comparison and Clarification of China and US CCUS Technology Development. Atmosphere, 2022, 13(12): 2114. (Reference to a journal publication)

[6] LI J. Accelerate the offshore CCUS to carbon-neutral China. Fundamental Research, 2022: S2667325822004289. (Reference to a journal publication)

[7] JIUTIAN Z, ZHIYONG W, JIA-NING K, et al. Several key issues for CCUS development in China targeting carbon neutrality. Carbon Neutrality, 2022, 1(1): 17. (Reference to a journal publication)

[8] 胡文瑞.中国低渗透油气的现状与未来.中国工程科学,2009,11(08):29-37. (Reference to a journal publication)

[9] BRADSHAW J, BACHU S, BONIJOLY D, et al. Task Force for Review and Identification of Standards for CO2 Storage Capacity Measurement. (Reference to a journal publication)

[10] AMPOMAH W, BALCH R, CATHER M, et al.

Evaluation of CO_2 Storage Mechanisms in CO_2 Enhanced Oil Recovery Sites: Application to Morrow Sandstone Reservoir. Energy & Fuels, 2016, 30(10): 8545-8555. (Reference to a journal publication)
[11] ASKAROVA A, MUKHAMETDINOVA A, MARKOVIC S, et al. An Overview of Geological CO2 Sequestration in Oil and Gas Reservoirs. Energies, 2023, 16(6): 2821. (Reference to a journal publication)
[12] JIA W, MCPHERSON B J, PAN F, et al. Probabilistic analysis of CO2 storage mechanisms in a CO2-EOR field using polynomial chaos expansion. International Journal of Greenhouse Gas Control, 2016, 51: 218-229. (Reference to a journal publication)
[13] YORDKAYHUN S, TRYGGVASON A, NORDEN B, et al. 3D seismic traveltime tomography imaging of the shallow subsurface at the C O2 SINK project site, Ketzin, Germany. GEOPHYSICS, 2009, 74(1): G1-G15. (Reference to a journal publication)
[14] LAWTON D, ALSHUHAIL A, COUESLAN M, et al. Pembina Cardium CO2 Monitoring Project, Alberta, Canada: Timelapse seismic analysis—Lessons learned. Energy Procedia, 2009, 1(1): 2235-2242. (Reference to a journal publication)
[15] HOVORKA S D, BENSON S M, DOUGHTY C, et al. Measuring permanence of CO2 storage in saline formations: the Frio experiment. Environmental Geosciences, 2006, 13(2): 105-121. (Reference to a journal publication).
[16] FAN M, LU D, LIU S. A deep learning-based direct forecasting of CO2 plume migration. Geoenergy Science and Engineering, 2023, 221: 211363. (Reference to a journal publication)
[17] DEFLANDRE J P, ESTUBLIER A, BARONI A, et al. Assessing Field Pressure and Plume Migration in CO2 Storages: Application of Case-specific Workflows at in Salah and Sleipner. Energy Procedia, 2013, 37: 3554-3564. (Reference to a journal publication)
[18] ZHENG X, ESPINOZA D N, VANDAMME M, et al. CO2 plume and pressure monitoring through pressure sensors above the caprock. International Journal of Greenhouse Gas Control, 2022, 117: 103660. (Reference to a journal publication)
[19] GEISTLINGER H, MOHAMMADIAN S. Capillary trapping mechanism in strongly water wet systems: Comparison between experiment and percolation theory. Advances in Water Resources, 2015, 79: 35-50. (Reference to a journal publication)
[20] KRISHNAMURTHY P G, TREVISAN L, MECKEL T. Investigating the Influence of Geological Heterogeneity on Capillary Trapping of Buoyant CO2 Using Transmitted-light Flow Visualization Experiments. Energy Procedia, 2017, 114: 4961-4966. (Reference to a journal publication)
[21] REN B. Local capillary trapping in carbon sequestration: Parametric study and implications for leakage assessment. International Journal of Greenhouse Gas Control, 2018, 78: 135-147. (Reference to a journal publication)
[22] NI H, MØYNER O, KURTEV K D, et al. Quantifying CO2 capillary heterogeneity trapping through macroscopic percolation simulation. Advances in Water Resources, 2021, 155: 103990. (Reference to a journal publication)
[23] ZHANG W, LI Y, OMAMBIA A N. Reactive transport modeling of effects of convective mixing on long-term CO2 geological storage in deep saline formations. International Journal of Greenhouse Gas Control, 2011, 5(2): 241-256. (Reference to a journal publication)
[24] HU H, XING Y, LI X. Self-diffusivity, M–S and Fick diffusivity of CO2 in Na-clay: The influences of concentration and temperature. Scientific Reports, 2017, 7(1): 5403. (Reference to a journal publication)
[25] AMARASINGHE W, FJELDE I, GUO Y. CO2 dissolution and convection in oil at realistic reservoir conditions: A visualization study. Journal of Natural Gas Science and Engineering, 2021, 95: 104113. (Reference to a journal publication)
[26] ZHANG G, LU P, HUANG Y, et al. Investigation of mineral trapping processes based on coherent front propagation theory: A dawsonite-rich natural CO2 reservoir as an example. International Journal of Greenhouse Gas Control, 2021, 110: 103400. (Reference to a journal publication)
[27] MISHRA A, BOON M M, BENSON S M, et al. Reconciling predicted and observed carbon mineralization in siliciclastic formations. Chemical Geology, 2023: 121324. (Reference to a journal publication)
[28] XU T, APPS J A, PRUESS K. Mineral sequestration of carbon dioxide in a sandstone–shale system. Chemical Geology, 2005, 217(3-4): 295-318. (Reference to a journal publication)
[29] KLEIN E, DE LUCIA M, KEMPKA T, et al. Evaluation of long-term mineral trapping at the Ketzin pilot site for CO2 storage: An integrative approach using geochemical modelling and reservoir simulation. International Journal of Greenhouse Gas Control, 2013, 19: 720-730. (Reference to a journal publication)